Instability Seeding Mechanisms due to Internal Defects in Inertial Confinement Fusion Targets

S. C. Miller and V. N. Goncharov

Laboratory for Laser Energetics and Department of Mechanical Engineering, University of Rochester

Performance degradation in laser-driven inertial confinement fusion implosions is caused by several effects, one of which is Rayleigh–Taylor instability growth. Target imperfections from manufacturing processes create instability seeds in the form of roughness or isolated "dome" features on the outer surface, gaps or separation between material layers, ice-layer roughness, and internal defects such as voids and bubbles. Additionally, tritium decay from the DT fuel can deposit energy into the ablator and DT ice layers and cause localized swelling in the plastic ablator material.1 A comprehensive understanding of seeding mechanisms is essential to characterize the impact of target defects on in-flight shell integrity and mass injection into the central, lower-density vapor region. An analysis of early-time behavior of both single-mode shell mass modulations and isolated voids is performed by examining the evolution of the acoustic waves launched by these target imperfections. A systematic study of localized perturbation growth as a function of defect placement and size is presented. The use of low-density ablator materials (such as foams) is suggested as a potential mitigation strategy to improve target robustness against the impact of defect-initiated growth.

A new parallel high-order multiphysics code (*Cygnus*[2]) is used to simulate internal ("bulk") perturbations inside the solid-density DT ice and plastic ablator materials. Perturbations are applied to planar 2-D foils (driven by a laser-like heat flux up to the start the acceleration phase) to study hydrodynamic wave propagation and seeding mechanisms at the ablation front. Convergence effects are not significant in early-time evolution, and the use of planar foils simplifies the analysis.

The foils used in this work are defined by three fluid regions: a 100-μm-thick, low-density $\rho = 0.001$-g/cm^3 layer representing the vapor region; a 40-μm-thick, $\rho = 0.25$-g/cm^3 layer representing DT ice; and an 8-μm-thick, heavier-density $\rho = 1$-g/cm^3 layer to mimic the plastic (CH) ablator. Density perturbations are applied in two forms: single-mode sinusoidal (to study basic seeding mechanisms) and isolated Gaussian voids (to closer mimic a realistic defect).

Figure 1 shows the trajectories of the ablation front, CH–DT interface, DT gas–ice interface, and two shocks created by the single-picket laser pulse (plotted in the lower pane). When shocks pass through an internal perturbation, such as a defect, a void in the material, or an interfacial gap, perturbation waves are launched that travel along characteristic hypersurfaces. For small perturbations decomposed into Fourier harmonics, each wave harmonic travels along characteristics defined as $(\mathrm{d}x/\mathrm{d}t)_{C^+} = U + c_s$ (the C^+ characteristic), as $(\mathrm{d}x/\mathrm{d}t)_{C^-} = U - c_s$ (the C^- characteristic), and $(\mathrm{d}x/\mathrm{d}t)_e = U$ (the entropy wave that travels with the local fluid velocity), where U is local fluid velocity and c_s is local sound speed. These characteristic trajectories define how perturbations propagate throughout the target and deposit seeds for instability growth. In the event of a shock-perturbation interaction, the C^+ characteristic wave carries the information back to the ablation front, the C^- characteristic wave catches up to and perturbs the shock front, and the entropy wave travels with the original defect (and defines the trajectory of the shock-induced vorticity).

Figure 2 shows the results from single-mode sinusoidal perturbations applied at various depths in the ice and ablator material of the foil. These depths are reported as relative to the CH–DT interface (where a positive value denotes a position inside the ablator material). Figure 2 plots the evolution of the distortion amplitude (peak to valley) of the ablation front due to perturbations with a single-mode wavelength of 100 μm. The time history of the ablation-front distortion shows the arrival of particular hydrodynamics waves such as shocks, rarefaction waves, and other characteristic waves. The two perturbations that start in the

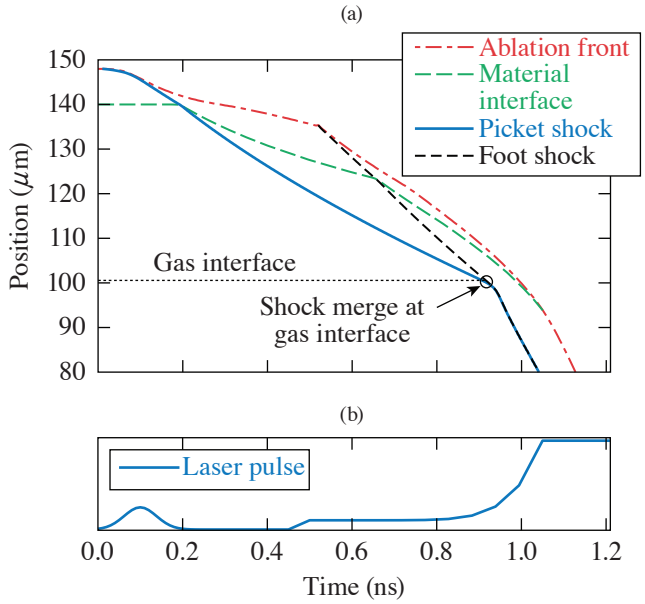

Figure 1
Interface and shock trajectories (position versus time) for the target and laser pulse.

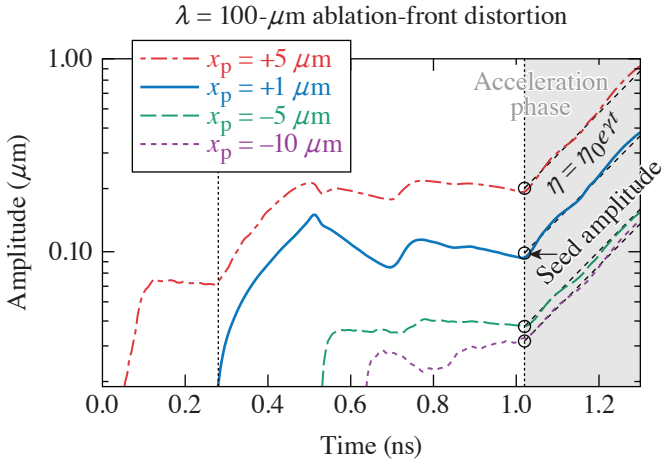

Figure 2
Ablation-front distortion history corresponding to perturbations at different locations in the ablator and DT ice. The acceleration phase is shaded in light gray. The dashed line is the exponential fit to $\eta = \eta_0 e^{\gamma t}$, and the seed amplitude is extracted from this curve. The initial perturbation depths (x_p) are +5, +1, –5, and –10 μm relative to the CH–DT interface for the red, blue, green, and purple lines, respectively. The vertical dotted black line near t = 0.3 ns indicae the arrival of the rarefaction wave at the ablation front.

ablator (red and blue curves) show significantly larger growth due to the rarefaction wave created by the interaction of the first shock (from the picket) and the CH-DT interface. This feedout growth process causes perturbations that start in the ablator to create larger seeds for instability growth when compared to those that originate in the ice. These seeds are defined as the amplitude of the distortion at the ablation front at the start of the acceleration phase (after which exponential RT growth occurs, or $\eta \sim \eta_0 e^{\gamma t}$, where γ is the growth rate and η is distortion). Figure 3 summarizes the seed amplitude (η_0) for perturbation wavelengths from 5 to 100 μm at different depths within the target material and shows the trend that perturbation seeds are largest when defects originate in the ablator and reduce as the initial position moves farther into the ice. As the wavelength reduces, however, interactions like destructive interference and phase change create wavelength-dependent behavior that complicates the position versus seed amplitude relationship. One region of particular interest [in Fig. 3(b)] is just inside of the CH–DT interface (near $x_p = -5$ μm). Here the interaction of the distorted CH–DT interface effectively cancels out or delays the onset of distortion growth at the ablation front (and reduces the acceleration-phase seed).

Simulations of isolated defects create complex wave interactions more likely to mimic target manufacturing defects, but much of the trends from single-mode perturbations apply. Figure 4(a) shows the density contour of the foil after the second shock has passed through a 1-μm defect (in the ablator). The black contour lines show velocity in the y direction and help to highlight

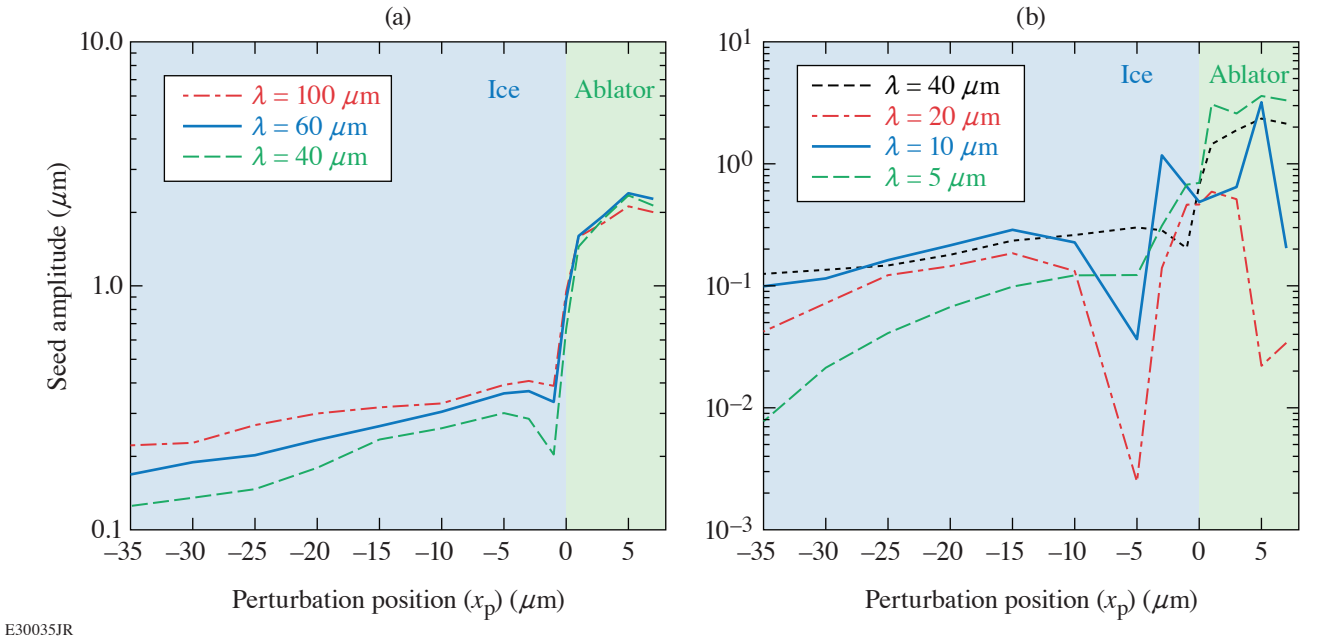

Figure 3
Scaled seed amplitudes as a function of perturbation position for (a) long-wavelength ($\lambda \geq 40$-mm) and (b) short wavelength ($\lambda < 40$-mm), single-mode perturbations.

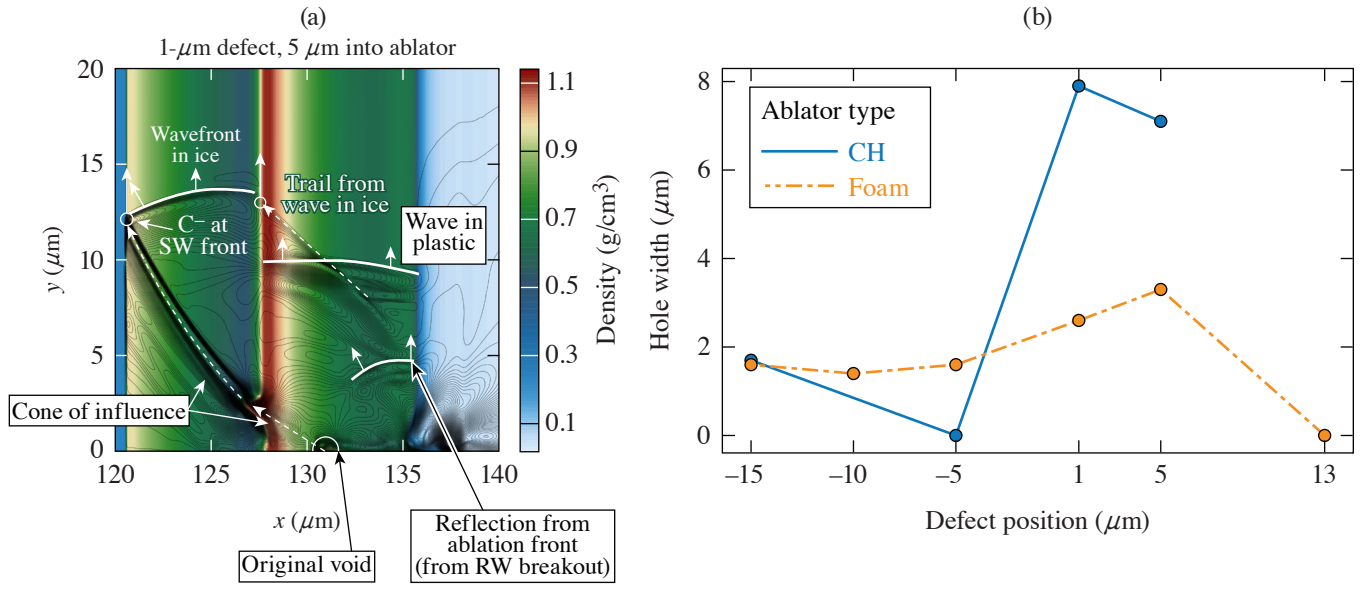

Figure 4
(a) Wave evolution for an isolated ablator defect (5 μm into the ablator from the CH–DT interface) at 0.5 ns after the first shock passage. Evolution in the y direction contributes to an extension of the maximum perturbation in y compared to the initial defect size. The contour colors show density and contour black lines show y velocity. (b) Hole sizes from shell punctures as a result of isolated defects in CH and wetted-foam targets approximately 300 ps after the start of the acceleration phase. RW: rarefaction wave; SW: shock wave.

particular wave features. These features include the wavefronts propagating through the different materials (ice and CH) and the lateral expansion of the defect perturbation. The lateral propagation is a unique feature of isolated defects (compared to sinusoidal perturbations). Isolated defect simulations show significant shell mass modulations and punctures at the start of the acceleration phase, depending on the position and size of the defect. Figure 4(b) shows the width of the hole due to a 1-μm defect located at various positions in the ice and ablator. Here, the degradation effects mimic the trend from short-wavelength, single-mode perturbations; ablator defects are more detrimental, and the effect is reduced just inward of the CH–DT interface.

A surrogate model that uses a wetted-foam ablator is proposed as a potential mitigation strategy to minimize the effects of manufacturing defects. In this design, the density is reduced from 1.0 (for CH) to 0.3 g/cm^3, and the shell thickness is increased to 26.7 μm (up from 8 μm) to conserve total shell mass compared to the CH ablator design. The smaller density reduces the strength of the rarefaction wave that travels from the ablator–ice interface (this rarefaction wave creates the large feedout growth shown in Fig. 1), and the increased thickness is beneficial because it isolates the defect perturbation (similar to how ice defects evolve). This effect can be seen in Fig. 4(b), where the foam ablator shows an overall reduction in hole width created by the defect.

Future work will examine internal defect evolution in 3-D and will include additional effects like convergent geometry along with and a more-detailed treatment of the materials (material-specific equations of state, radiation opacity, multiple materials, etc.). Additional work will seek to optimize shell thickness and continue to study alternative foam-like ablator designs.

This material is based upon work supported by the Department of Energy National Nuclear Security Administration under Award Number DE-NA0003856, the University of Rochester, and the New York State Energy Research and Development Authority.

1. D. R. Harding and W. T. Shmayda, Fusion Sci. Technol. **63**, 125 (2013).
2. S. C. Miller, "Hydrodynamic Instabilities in Inertial Confinement Fusion: Physics, Numerical Methods, and Implementation," Ph.D. Thesis, University of Rochester, 2022.